Synthesis of matched magnetic fields for controlled spin precession

Louis-S. Bouchard[1,*] and M. Sabieh Anwar[1,2]
[1]*Materials Sciences Division, Lawrence Berkeley National Laboratory and Department of Chemistry, University of California, Berkeley, California 94720, USA*
[2]*School of Science and Engineering, Lahore University of Management & Sciences (LUMS), Pakistan*
(Received 7 February 2007; revised manuscript received 7 April 2007; published 26 July 2007)

The shaping of magnetic fields is important in many areas of physics, including magnet shimming, electromagnetic traps, magnetic domain switching, and controlled spin precession in nuclear magnetic resonance (NMR). We examine the method of target field matching by orthogonal projection and its application to NMR, whereby the phase of nuclear spins in a strongly inhomogeneous field is corrected through stroboscopic ac irradiation using matching fields. Three-dimensional shaping of static and ac fields can restore the spectral resolution by orders of magnitude using simple linear combinations of a small number of independent sources. Results suggest the possibility of substantially pushing the current limits of high-resolution NMR spectroscopy in weak and inhomogeneous fields. We also discuss conditions under which concomitant gradient effects are important in high magnetic fields and the geometric-phase errors they introduce during precession in ac fields.

DOI: 10.1103/PhysRevB.76.014430 PACS number(s): 76.60.Jx, 82.56.Lz, 07.57.Pt, 07.55.Db

I. INTRODUCTION

In many situations, it is crucial to shape a magnetic field both in amplitude and in direction. Unlike the electric field, the magnetic field is generally more difficult to "sculpt" because of the absence of magnetic monopoles. In recent years, this problem has acquired more prominence with the need for miniaturized, high-speed magnetic devices.[1] In magnetic recording, the magnetization reversal of a ferromagnetic body can be done using the torque on magnetization $\mathbf{B}\times\mathbf{M}$ (precessional switching) or the unbalance of energies $\mathbf{B}\cdot\mathbf{M}$ of the initial and reversed magnetization positions. In both cases, the strength and direction of the magnetic field with respect to $\mathbf{M}$ are critical for optimal performance.[1–3]

Another fundamental physical application is the understanding of spin-wave excitation in small magnetic elements, whereby quantized and localized spin-wave eigenmodes depend nontrivially on element shape and internal static or dynamic field inhomogeneity.[1–3] Magnetic resonance force microscopy also relies on shaped magnetic-field gradients for the spatial localization of nuclear or electronic spin precession. Furthermore, shaped static and radio-frequency fields permit the effective trapping of ions in electromagnetic traps.[4] Within enclosed volumes, these fields can be synthesized using surfaces machined to high precision[4,5] or with coils producing spatially orthogonal fields.[6]

The present paper addresses the general problem of designing precise magnetic fields with desired magnitude and directional profiles. Our main motivation is in the context of NMR. This popular form of two-level coherent spectroscopy[7,8] has the primary goal of extracting high-resolution spectra that carry precise molecular and structural information about the sample of interest. The spins at position $\mathbf{r}$ precess at the Larmór frequency, which is determined by the sum of electronic screening effects (chemical shift) and the magnetic field $\mathbf{B}(\mathbf{r})$. The NMR signal is the volume integral over the sample volume or over a voxel. For sufficiently inhomogeneous $\mathbf{B}(\mathbf{r})$, chemical shift information may be completely obscured, making it difficult or impossible to extract useful structural information of a compound to be analyzed. This is the main problem encountered with the one-sided magnet geometries of portable NMR sensors.[9–11] Some level of magnetic-field synthesis, or "matching," is an absolute requirement for truly *ex situ* or mobile nuclear resonance methods.

A method for counteracting the phase decoherence in inhomogeneous static fields, termed B_0-B_1 matching, has already been demonstrated using inhomogeneous radio-frequency (rf) fields.[12–15] The method significantly improves the effective field homogeneity, enabling one to recover high-resolution NMR spectra in the presence of inhomogeneities. The essence of the matching method[15] is as follows. The time-independent field $\mathbf{B}_0(\mathbf{r})$ is a sum of uniform and nonuniform components, $\mathbf{B}_0(\mathbf{r})=\mathbf{B}_0+\delta\mathbf{B}_0(\mathbf{r})$. Transformation to the interaction representation leaves only the nonuniform component $\delta\mathbf{B}_0(\mathbf{r})$ to be compensated for. This is precisely the term responsible for introducing destructive interference in the spin phases.

We may envisage two ways in which the effect of $\delta\mathbf{B}_0(\mathbf{r})$ can be counteracted. First, using synthesized stroboscopic ac fields to correct for the phase dispersion accrued due to $\delta\mathbf{B}_0(\mathbf{r})$, and second, using a synthesized dc corrective field of the form $-\delta\mathbf{B}_0(\mathbf{r})$. These two methods will be exemplified in Secs. IV A and IV B of this paper, where we treat an important extension to the matching method. The first approach using ac fields has the advantage that weaker inhomogeneities can be used to correct the effects of large inhomogeneities.

We investigate the method of orthogonal projections of magnetic-field sources for matching arbitrary field distributions. The only requirement is linear independence of the source fields and, unlike conventional shimming methods,[6] it does not require the cumbersome hardware requirements of special coil designs that produce orthonormal fields. The method can be used for correcting (or for purposely introducing) static field as well as rf field inhomogeneities. In particular, we show that in a ~1-T static field, it is possible to correct over a frequency spread $\delta B_0/(\gamma/2\pi)$ of up to

50 kHz (γ is the magnetogyric ratio of the nuclei). Furthermore, the procedure corrects for magnetic-field gradient polynomials of arbitrary order. These results are more than an order of magnitude improvement over published methods.[15]

Besides magnetic-field inhomogeneities, another important consideration in synthesizing desired field distributions is the presence of concomitant fields.[16–18] It was previously assumed[18–20] that the effect of these components is significant only in low fields. In the present paper, we show their importance in high fields and present ways of avoiding unwanted perturbations to the quantum evolution of the nuclear spins. This discussion is an extension of a previous paper,[21] which showed that the effects of concomitant components in MRI can be described by the concept of geometric-phase errors.

II. FIELD MATCHING

A. Matching conditions

The magnetic field in current-free regions is subject to the fundamental conditions on its differentiability, $\nabla \times \mathbf{B}(\mathbf{r})=0$, and $\nabla \cdot \mathbf{B}(\mathbf{r})=0$, which impose fundamental constraints on the components of the gradient tensor,

$$\nabla \mathbf{B}(\mathbf{r}) = \frac{\partial B_i}{\partial r_j}(\mathbf{r}). \tag{1}$$

These relations imply that $\nabla \mathbf{B}$ is a traceless symmetric tensor and therefore has only five independent components, i.e., it is a pure rank-2 spherical tensor. When a target magnetic field is crafted to a desired field profile, it is important that the synthesis accounts for all the components of $\partial B_i / \partial r_j$ unless the transformation to the interaction representation results in the time-averaging of some components.

The use of rf (Ref. 15) and static[22] gradient fields has been proposed to unwind the decoherence of spin phases in an inhomogeneous field. In particular, the approach outlined by Meriles and co-workers[15,23] imposes a $\mathbf{B}_1(\mathbf{r})$ field which matches $\mathbf{B}_0(\mathbf{r})$ in the scalar sense, i.e., the magnitudes are proportional,

$$\delta B_0(\mathbf{r}) = k \delta B_1(\mathbf{r}), \tag{2}$$

up to an arbitrary parameter-free scaling factor k. If we assume that the static field nonuniformity is along z, the rf field will be applied along an orthogonal axis, say x,

$$\delta B_{0,z}(\mathbf{r}) = k \delta B_{1,x}(\mathbf{r}). \tag{3}$$

The rf field creates a Hamiltonian that can reverse the Zeeman precession of the spins in the static gradient, under the free evolution Hamiltonian *while preserving evolution under chemical shielding frequency offset*. This is a remarkable observation, considering the fact that the irreducible tensor operators for chemical shift and Zeeman evolutions have the same transformation properties under rotations. The Meriles method accomplishes the phase compensation with a three-pulse composite rotation to be described later.

The relation of Eq. (3) is not completely general; it explicitly enforces the desirable constraint that the matching rf field has a null concomitant component,

$$\delta B_{0,z}(\mathbf{r}) = k \delta B_{1,x}(\mathbf{r}), \quad \text{with } B_{1,y} = 0, \tag{4}$$

for, without this concomitant field nulling, serious problems may arise unless additional precautions are taken. More often than not, these concomitant components in the rotating frame during rf induced nutation are unjustifiably ignored. We show that their presence can lead to serious geometric-phase errors and distortions during Fourier encoding unless $B_{1,y}$ is explicitly nulled or that a constant offset is added to $\mathbf{B}_1$ that is much larger and therefore truncates the gradient in $\mathbf{B}_1$, i.e., the condition $\max_{\mathbf{r}\in\mathcal{V}} |\delta \mathbf{B}_1(\mathbf{r})| / |\mathbf{B}_1| \ll 1$ in the target volume $\mathcal{V}$ is satisfied. In Appendix A, we give a more general matching condition based on a differential-geometric interpretation of the magnetic-field nonuniformities.

B. Field synthesis by orthogonal projection

In what follows, the optimization volume of interest is designated $\mathcal{V} \subset \mathbb{R}^3$. This is the region over which the field matching is to be performed. We define an inner product of two vector-valued functions, $\mathbf{B}_1$ and $\mathbf{B}_2$, whose components are real-valued and square integrable,

$$(\mathbf{B}_1, \mathbf{B}_2) = \int_{\mathcal{V}} \mathbf{B}_1(\mathbf{r}) \cdot \mathbf{B}_2(\mathbf{r}) d^3\mathbf{r}, \tag{5}$$

where $\mathbf{B}_1 \cdot \mathbf{B}_2$ denotes the usual scalar product of two vectors $\mathbf{B}_1$ and $\mathbf{B}_2$ in $\mathbb{R}^3$. With an inner product $(\cdot, \cdot)$, the norm of $\mathbf{B}$ can always be taken to be the induced norm, $\|\mathbf{B}\| = \sqrt{(\mathbf{B}, \mathbf{B})}$. We may also include an everywhere positive kernel, $h(\mathbf{r}) > 0$, which multiplies the integrand. The kernel $h(\mathbf{r})$ may be used to emphasize or de-emphasize different regions of $\mathcal{V}$ according to their importance. A useful kernel is a three-dimensional (3D) Gaussian function which emphasizes the central region and attributes less importance to the edges. In the present work, we use both the Gaussian and the uniform kernels.

We consider a set of n linearly independent magnetic fields $\{\mathbf{B}_1, \mathbf{B}_2, \ldots, \mathbf{B}_n\}(\mathbf{r})$ (vector-valued functions defined on some domain in $\mathbb{R}^3$). When the n fields are operated in ac mode, the magnetic field $\mathbf{B}_i$ refers to the time-independent part of the field $\mathbf{B}_i(t) = \mathbf{B}_i \cos(\omega_i t)$. By assigning a weighting factor a_i to each available field and summing $\Sigma_{i=1}^n a_i \mathbf{B}_i(\mathbf{r})$, an arbitrary function $\mathbf{B}$ can be matched by adjusting the set of weights $\{a_i\}$ in a least-squares optimal manner. This gives the best mean-square estimator of $\mathbf{B}$ in the linear manifold $\mathcal{L}\{\mathbf{B}_1, \ldots, \mathbf{B}_n\}$.

Let $\{\tilde{\mathbf{B}}_1, \ldots, \tilde{\mathbf{B}}_n\}$ be an orthonormal system and $\mathbf{B}$ any vector-valued function in a bounded region $\mathcal{V} \subset \mathbb{R}^3$ whose components are square-integrable functions. The inequality

$$\left\| \mathbf{B} - \sum_{i=1}^{n} a_i \tilde{\mathbf{B}}_n \right\|^2 \geqslant \|\mathbf{B}\|^2 - \sum_{i=1}^{n} |(\mathbf{B}, \tilde{\mathbf{B}}_i)|^2 \tag{6}$$

implies that the infimum of $\|\mathbf{B} - \Sigma_{i=1}^n a_i \tilde{\mathbf{B}}_i\|^2$ over all real $a_1, \ldots, a_n$ is attained for $a_i = (\mathbf{B}, \tilde{\mathbf{B}}_i)$, $i = 1, \ldots, n$. Consequently, the best estimator[44] for $\mathbf{B}$ in terms of $\tilde{\mathbf{B}}_1, \ldots, \tilde{\mathbf{B}}_n$ is

$$\hat{\mathbf{B}} = \sum_{i=1}^{n} a_i \tilde{\mathbf{B}}_i = \sum_{i=1}^{n} (\mathbf{B}, \tilde{\mathbf{B}}_i)\tilde{\mathbf{B}}_i. \tag{7}$$

If the sequence $\{\mathbf{B}_1, \ldots, \mathbf{B}_n\}$ is not an orthonormal system, we may use the Gram-Schmidt orthonormalization procedure to obtain an orthonormal sequence $\{\tilde{\mathbf{B}}_1, \ldots, \tilde{\mathbf{B}}_n\}$. The orthogonalization procedure may be cast into a matrix transformation,

$$\tilde{\mathbf{B}}_i = \sum_{j=1}^{n} \mathsf{T}_{ij} \mathbf{B}_j, \tag{8}$$

where T_{ij} is an invertible matrix with inverse denoted by V_{ij} ($\mathbf{V}=\mathbf{T}^{-1}$).

Next, the relative weights of each field $\hat{\mathbf{B}}_i$ are calculated as follows. The estimator with coefficients $\mathbf{a}=\{a_1, \ldots, a_n\}$ of the orthogonal fields $\tilde{\mathbf{B}}_i$ equals the physical fields $\mathbf{B}_i$ weighted by coefficients $\mathbf{w}=\{w_1, \ldots, w_n\}$,

$$\sum_{i=1}^{n} a_i \tilde{\mathbf{B}}_i = \sum_{i=1}^{n} w_i \mathbf{B}_i = \sum_{i=1}^{n} w_i \sum_{j=1}^{n} V_{ij} \tilde{\mathbf{B}}_j. \tag{9}$$

Equating the coefficients of the $\tilde{\mathbf{B}}_i$ gives the system of equations $\mathbf{a}=\mathbf{V}\mathbf{w}$ which upon inversion gives $\mathbf{w}=\mathbf{T}\mathbf{a}$, and we have the relative weights $\mathbf{w}$ of each field given in terms of some orthogonalization matrix and the coefficients $\mathbf{a}$ of the mean-square estimator.

III. EFFECTS OF CONCOMITANT GRADIENTS IN SPATIALLY VARYING ac FIELDS

Equipped with a method for crafting arbitrary magnetic fields that match a target field, we now implement the matching approach[15] of using a spatially varying ac field, say $B_{1,x}(\mathbf{r})$. We must first determine the effects of the concomitant component, $B_{1,y}(\mathbf{r})$, and establish the conditions, if they exist, under which it can be neglected.

A. Spin excitation

The first step in most NMR (and imaging) experiments is spin excitation, which subsequently enables the acquisition of a spectrum, or for the imaging case, spatial encoding.[24] For an ac field with carrier frequency ω_c, the part of the Hamiltonian which describes the interaction of the spin with the classical radiation field is

$$\mathcal{H}_1 = \gamma[B_{1,x}(\mathbf{r})I_x + B_{1,y}(\mathbf{r})I_y + B_{1,z}(\mathbf{r})I_z]\cos(\omega_c t + \varphi), \tag{10}$$

where γ is the magnetogyric ratio, I_α, $\alpha=x,y,z$ are the Cartesian spin angular momentum operators, which for a single spin 1/2 are rescaled Pauli spin matrices, $I_\alpha=\sigma_\alpha/2$,[25] and the field $\mathbf{B}_1=(B_{1,x},B_{1,y},B_{1,z})(\mathbf{r})$ includes all spatial gradients. These rf field gradients are important for several applications, including imaging, diffusion measurements, and NMR microscopy, and are known to be immune to susceptibility inhomogeneities.[26–28] Transforming Eq. (10) to the interaction representation using the unitary operator $V=\exp(-i\omega_0 I_z t)$, where ω_0 is the Larmór frequency, gives

$$\begin{aligned}\tilde{\mathcal{H}}_1/\gamma = {} & B_{1,x}(\mathbf{r})\cos(\omega_c t + \varphi)\cos\,\omega_0 t\, I_x \\ & - B_{1,x}(\mathbf{r})\cos(\omega_c t + \varphi)\sin\,\omega_0 t\, I_y \\ & + B_{1,y}(\mathbf{r})\cos(\omega_c t + \varphi)\cos\,\omega_0 t\, I_y \\ & + B_{1,y}(\mathbf{r})\cos(\omega_c t + \varphi)\sin\,\omega_0 t\, I_x \\ & + B_{1,z}(\mathbf{r})\cos(\omega_c t + \varphi) I_z. \end{aligned} \tag{11}$$

Substituting $\Delta\omega=\omega_c-\omega_0$ and expanding,

$$\begin{aligned}\tilde{\mathcal{H}}_1/\gamma = {} & \frac{B_{1,x}(\mathbf{r})}{2}\{\cos(\Delta\omega t + \varphi) + \cos[(\omega_c + \omega_0)t + \varphi]\} I_x \\ & - \frac{B_{1,x}(\mathbf{r})}{2}\{\sin[(\omega_c + \omega_0)t + \varphi] - \sin[\Delta\omega t + \varphi]\} I_y \\ & + \frac{B_{1,y}(\mathbf{r})}{2}\{\cos[(\omega_c + \omega_0)t + \varphi] + \cos[\Delta\omega t + \varphi]\} I_y \\ & + \frac{B_{1,y}(\mathbf{r})}{2}\{\sin[(\omega_c + \omega_0)t + \varphi] - \sin[\Delta\omega t + \varphi]\} I_x \\ & + B_{1,z}(\mathbf{r})\cos(\omega_c t + \varphi) I_z. \end{aligned} \tag{12}$$

In high fields, the terms oscillating at the rf carrier frequency ω_c and at the sum of frequencies $\omega_c+\omega_0$ rapidly average to zero,

$$\begin{aligned}\tilde{\mathcal{H}}_1(2/\gamma) = {} & [B_{1,x}(\mathbf{r})\cos(\Delta\omega t + \varphi) - B_{1,y}(\mathbf{r})\sin(\Delta\omega t + \varphi)] I_x \\ & + [B_{1,x}(\mathbf{r})\sin(\Delta\omega t + \varphi) + B_{1,y}(\mathbf{r})\cos(\Delta\omega t + \varphi)] I_y. \end{aligned} \tag{13}$$

In this expression, the spatial dependence is carried by the terms $\Delta\omega \equiv \Delta\omega(\mathbf{r})$ and $\mathbf{B}_1(\mathbf{r})$. The spatial dependence of $\Delta\omega$ is due to the Larmór frequency, which is itself a function of position. For on-resonance irradiation, $\Delta\omega=0$, and if additionally the phase $\varphi=0$, the Hamiltonian reduces to

$$\tilde{\mathcal{H}}_{1,\varphi=0} = \frac{\gamma}{2}[B_{1,x}(\mathbf{r})I_x + B_{1,y}(\mathbf{r})I_y], \tag{14}$$

while for $\varphi=\pi/2$ we have

$$\tilde{\mathcal{H}}_{1,\varphi=\pi/2} = \frac{\gamma}{2}[-B_{1,y}(\mathbf{r})I_x + B_{1,x}(\mathbf{r})I_y]. \tag{15}$$

Now let $B_{1,x}(\mathbf{r})$ be the intended field and consider the case of $\varphi=0$. Instead of a nutation about the desired I_x axis, we get a nutation about an axis that makes the spatially dependent angle $\tan^{-1}[B_{1,y}(\mathbf{r})/B_{1,x}(\mathbf{r})]$ with respect to I_x in the xy plane. A similar argument applies for the $\varphi=\pi/2$ case. Thus the concomitant field components $[B_{1,y}(\mathbf{r})$ for $\varphi=0$ and $B_{1,x}(\mathbf{r})$ for $\varphi=\pi/2]$ "contaminate" the intended rotation and can potentially lead to severe distortion of the spatial spin excitation profile.

B. Concomitant fields

The concept of "concomitant fields"[16–18] is a direct consequence of Maxwell's equations. In high-field magnetic

TABLE I. Examples of B_z fields and admissible concomitant components B_x and B_y.

Label	B_z	B_x	B_y
A	1	0	0
B	x	z	0
C	y	0	z
D	$-z$	$0.5y$	$0.5x$
E	xy	xz	yz
F	x^2-y^2	$2xz$	$-2yz$
G	0	x^3-3xy^2	$-3x^2y+y^3$
H	0	$x^4-6x^2y^2+y^4$	$-4x^3y+4xy^3$
I	0	$x^5-10x^3y^2+5xy^4$	$-5x^4y+10x^2y^3-y^5$
J	$1+x+y$ $-z+xy$ $+(x^2-y^2)$	$0.5x+z+yz+2xz$ $+x^3-3xy^2+x^4$ $-6x^2y^2+y^4+x^5$ $-10x^3y^2+5xy^4$	$0.5y+z+xz-2yz$ $-3x^2y+y^3-4x^3y$ $+4xy^3-5x^4y$ $+10x^2y^3-y^5$

resonance, the presence of concomitant fields has largely been ignored as their rapidly oscillating behavior in the interaction representation results in a time-averaged value of zero. This secular approximation is generally referred to as "truncation." In low magnetic fields, because the truncating Zeeman Hamiltonian is weak, the averaging is incomplete. These residual concomitant components can lead to distortions in spin phase.[16–18] Recently, these distortions have been shown to originate in the geometric (Berry) phase.[21]

These concomitant components are of concern when synthesizing a matching field for a given target field which is spatially varying. For example, to prescribe a field component $B_z=x^2-y^2$, the curl-free condition requires that $\partial_z B_y=\partial_y B_z$ and $\partial_z B_x=\partial_x B_z$. It is enough to take $B_x=2xz$ and $B_y=-2yz$ in order to obtain a physically realizable field. Some examples of B_z fields and their concomitant components are given in Table I.

C. Effect of concomitant components on universal Euler rotations

The contribution of concomitant gradients to the geometric-phase error leading to phase distortions is best quantified in terms of its effect on the general Euler rotation in SU(2). The generalized rotation operator is

$$R(\alpha,\beta,\gamma)=e^{-i\alpha I_z}e^{-i\beta I_y}e^{-i\gamma I_z}, \tag{16}$$

where α, β, and γ are the Euler angles[29] and spin operators are applied from left to right. In NMR the rotations usually take place in the xy plane, and the rotations about I_z are performed using the equivalent rotation,

$$e^{-i\alpha I_z}=e^{-i(\pi/2)I_y}e^{-i\alpha I_x}e^{i(\pi/2)I_y}, \tag{17}$$

and similarly for the γ rotation. Therefore the experimentally realized general Euler rotation operator consists of the following sequence of rotations:

$$e^{-i(\pi/2)I_y}e^{-i\alpha I_x}e^{i(\pi/2)I_y}e^{-i\beta I_y}e^{-i(\pi/2)I_y}e^{-i\gamma I_x}e^{i(\pi/2)I_y}. \tag{18}$$

In practice, I_x rotations are obtained by setting the pulse phase $\varphi=0$ while rotations about I_y use $\varphi=\pi/2$. In the presence of inhomogeneous fields, the I_x and I_y Hamiltonians are replaced by Eq. (13).

Consider the x component of an ac field whose magnitude in the interaction representation is $B_{1,x}(\mathbf{r})=B_{1,x}+\delta B_{1,x}(\mathbf{r})$, where $B_{1,x}$ is the constant part and $\delta B_{1,x}(\mathbf{r})$ is the nonuniform part, and suppose that it is desired to implement a rotation through an angle α. The concomitant field is $\delta B_{1,y}(\mathbf{r})$. For the intended nutation angle, the pulse duration obeys $\tau=2\alpha/\gamma B_{1,x}(\mathbf{r})$. This yields the experimentally realized rotation for on-resonance irradiation,

$$\begin{aligned}R'(\alpha,\beta,\gamma)=&\,e^{-i(\pi/2)[(1+\delta B_{1,x}/B_{1,x})I_y-(\delta B_{1,y}/B_{1,x})I_x]}\\&\times e^{-i\alpha[(1+\delta B_{1,x}/B_{1,x})I_x+(\delta B_{1,y}/B_{1,x})I_y]}\\&\times e^{i(\pi/2)[(1+\delta B_{1,x}/B_{1,x})I_y-(\delta B_{1,y}/B_{1,x})I_x]}\\&\times e^{-i\beta[(1+\delta B_{1,x}/B_{1,x})I_y-(\delta B_{1,y}/B_{1,x})I_x]}\\&\times e^{-i(\pi/2)[(1+\delta B_{1,x}/B_{1,x})I_y-(\delta B_{1,y}/B_{1,x})I_x]}\\&\times e^{-i\gamma[(1+\delta B_{1,x}/B_{1,x})I_x+(\delta B_{1,y}/B_{1,x})I_y]}\\&\times e^{i(\pi/2)[(1+\delta B_{1,x}/B_{1,x})I_y-(\delta B_{1,y}/B_{1,x})I_x]},\end{aligned} \tag{19}$$

which diverges from the Euler rotation $R(\alpha,\beta,\gamma)$ of Eq. (16) when $\delta B_{1,y}(\mathbf{r})\neq 0$. In magnetic resonance, the rotation operator in the presence of rf gradients is usually assumed to have no concomitant components $[\delta B_{1,y}(\mathbf{r})=0]$,

$$\begin{aligned}R_d(\alpha,\beta,\gamma)=&\,e^{-i(\pi/2)[(1+\delta B_{1,x}/B_{1,x})I_y]}e^{-i\alpha[(1+\delta B_{1,x}/B_{1,x})I_x]}\\&\times e^{i(\pi/2)[(1+\delta B_{1,x}/B_{1,x})I_y]}e^{-i\beta[(1+\delta B_{1,x}/B_{1,x})I_y]}\\&\times e^{-i(\pi/2)[(1+\delta B_{1,x}/B_{1,x})I_y]}e^{-i\gamma[(1+\delta B_{1,x}/B_{1,x})I_x]}\\&\times e^{i(\pi/2)[(1+\delta B_{1,x}/B_{1,x})I_y]}.\end{aligned} \tag{20}$$

This is certainly not true in the general case, even at high magnetic fields, where the concomitant gradients are normally ignored. We may describe these deviations of the experimental from the desired rotation operator, Eqs. (19) and (20), in terms of the projection of R' onto R_d, $F_R(\mathbf{r})=\mathrm{Tr}\,[R'^{\dagger}(\mathbf{r})R_d(\mathbf{r})]$. Since the rotation operators depend on position, we may use the volume average ($|\mathcal{V}|=\int_{\mathcal{V}}d^3\mathbf{r}$):

$$\langle F_R\rangle=\frac{1}{|\mathcal{V}|}\int_{\mathcal{V}}\mathrm{Tr}[R'^{\dagger}(\mathbf{r})R_d(\mathbf{r})]d^3\mathbf{r}. \tag{21}$$

Only in the limit of small concomitant fields $\delta B_{1,y}/B_{1,x}$ does the volume-averaged fidelity approach $\lim_{\delta B_{1,y}/B_{1,x}\to 0}\langle F_R\rangle=1$.

To illustrate the effect of concomitant gradients on general Euler rotations, consider the rotation $R(\alpha,\beta,\gamma)$, where $\alpha=10°$, $\beta=20°$, and $\gamma=30°$, in the presence of an applied inhomogeneous rf field,

$$\begin{aligned}B_{1,x}(\mathbf{r})=10+g[x(x^2-y^2)-2xy^2],\\-0.5\leqslant x\leqslant 0.5;-0.5\leqslant y\leqslant 0.5,\end{aligned} \tag{22}$$

where g is a constant. From Table I, the concomitant component is $B_{1,y}(\mathbf{r})=g\,[-2x^2y-y(x^2-y^2)]$. Figures 1(d)–1(f) show plots of the operator fidelity F_R corresponding to this

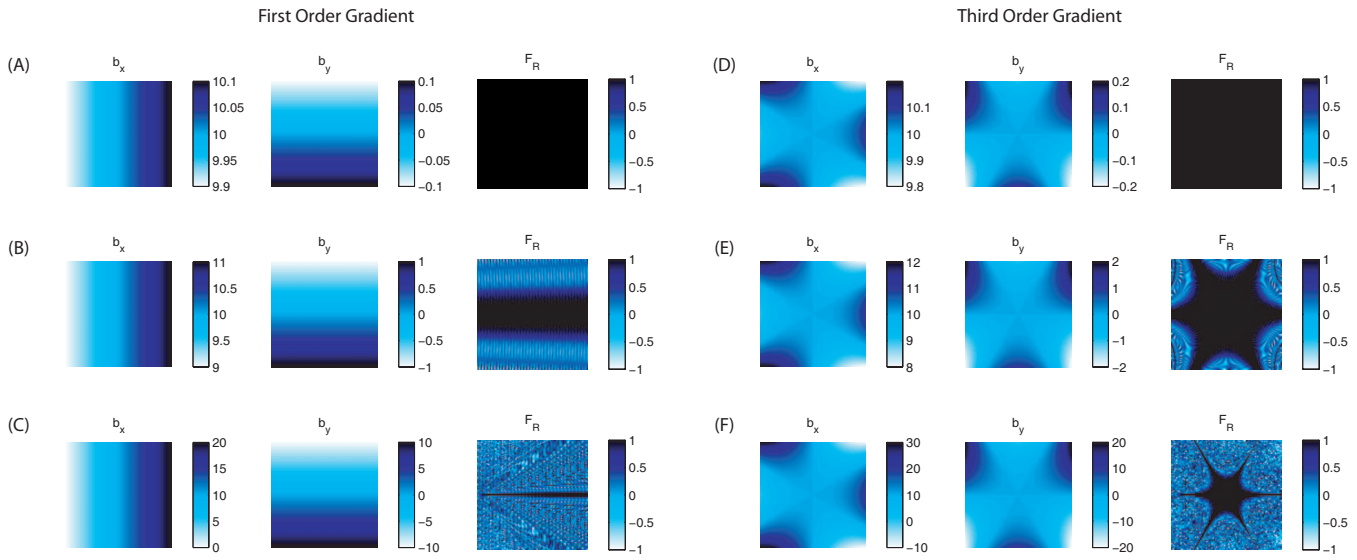

FIG. 1. (Color online) Effect of concomitant rf gradients on the operator fidelity F_R of the Euler rotation $(\alpha,\beta,\gamma)=(10°,20°,30°)$. In (A)–(C) we have $B_{1,x}(\mathbf{r})=10+gx$ and $B_{1,y}(\mathbf{r})=gy$, while in (D)–(F) we used $B_{1,x}(\mathbf{r})=10+g\ [x(x^2-y^2)-2xy^2]$, $B_{1,y}(\mathbf{r})=g\ [-2x^2y-y(x^2-y^2)]$ with $(x,y)\in[-0.5,0.5]\times[-0.5,0.5]$. Three values of the gradient strength are shown: (A),(D) $g=0.1$, (B),(E) $g=1.0$, and (C),(F) $g=10.0$.

gradient field as a function of (x,y), and for three different values of $g=0.1$, 1.0, and 10.0. We note that significant deviations from R_d arise at $g=1.0$ resulting in large signal losses. The deviations are even more pronounced in the case of a linear gradient, as shown in Figs. 1(a)–1(c), where more than half of the volume is lost to distorted rotations at $g=1.0$. This means that rf coils used to produce linear x gradients with zero dc offset must be designed to produce relatively weak concomitant gradients, i.e., $\max_{\mathbf{r}\in\mathcal{V}}|\delta B_{1,y}(\mathbf{r})|/|B_{1,x}|$ should be less than 0.1. Figure 2 shows the effects of concomitant ac gradients on MRI image acquisition. In the absence of an adequate dc offset, a gradient field large compared to the ac field amplitude causes severe image distortions.

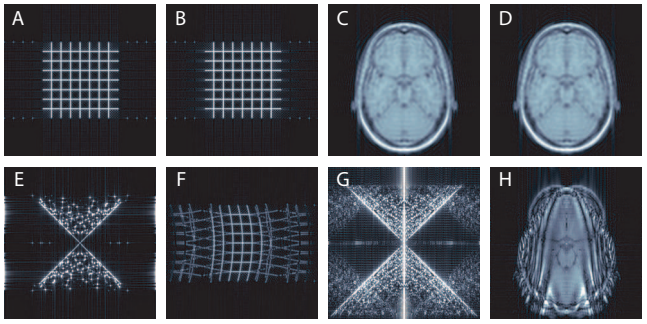

FIG. 2. (Color online) Effect of concomitant rf gradients on echo-planar magnetic-resonance images for (A), (B), (E), (F) a grid pattern and (C), (D), (G), (H) human brain. Images without any concomitant fields are shown in (A) and (C). At the edges of the field of view, the ratio of concomitant field to constant field $\delta B_{1,y}/B_{1,x}$ was (A) 0, (B) 1/25, (F) 1, and (E) ∞ for the grid. For the brain image, the ratios are (C) 0, (D) 1/50, (H) 1, and (G) ∞. A ratio of ∞ is obtained, for example, using a Golay or Maxwell pair gradient coil, where the dc component of the B_1 field is zero. A surface coil or solenoid, on the other hand, has a nonzero dc component everywhere.

We conclude that there are two possibilities for high fidelity excitation of nuclear spin transitions in inhomogeneous fields: The first approach uses a large position-independent field such that $\max_{\mathbf{r}\in\mathcal{V}}|\delta B_{1,y}(\mathbf{r})|/|B_{1,x}|<0.1$. The second approach requires fields with vanishing B_x or B_y components, according to whether the Hamiltonian of Eqs. (14) or (15) is used. In Appendix B, simple relations are given for constructing such fields.

IV. SPECTRAL LINE NARROWING

In this section, we investigate the performance of the orthogonal projection method to create a desired target field for use in magnet shimming and spin phase compensation. A possible physical realization is illustrated in Fig. 3. All calculations in this study are based on the flat coil array (Fig. 3) with Cartesian array of current loops, each with adjustable current. The volume of interest $\mathcal{V}$ is placed above the plane of the transmitter.

Using the inner product of magnetic fields, we define the field fidelity $\mathcal{F}$ $(-1\leqslant\mathcal{F}\leqslant 1)$,

$$\mathcal{F}=(\hat{\mathbf{B}},\mathbf{B})/\|\hat{\mathbf{B}}\|\|\mathbf{B}\|, \tag{23}$$

where the integral is taken over the volume of interest $\mathcal{V}$. The maximum value of 1 is attained in the limit $\hat{\mathbf{B}}\to\mathbf{B}$. Fidelities for some vector fields are presented in Table II. The data show that in some cases, we can approach fidelities very close to 1. Figure 4 shows some horizontal slices in the three-dimensional volume depicting the desired and actual estimated fields, illustrating the high degree of fidelity.

A. Quantal phase correction using ac field gradients

Good fidelities (>0.9) for the target field projector method indicate the ability to closely match arbitrary linear

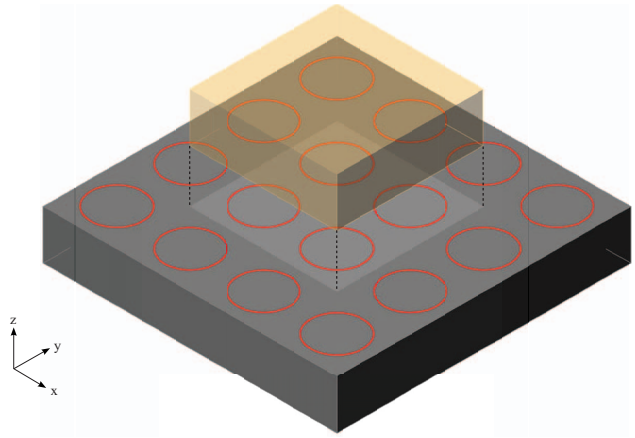

FIG. 3. (Color online) Cartesian-grid arrangement for a 4×4 single-sided array of magnetic-field sources on the surface of a one-sided transmitter. These sources are depicted as red circles. The target volume is a rectangular parallelepiped region located near the transmitter surface and is represented as the colored volume raised above the transmitter surface. For simulations, we assume an array surface area of 12×12 cm and a target volume region with dimensions 6×6 cm in the xy plane, 2 cm thick and positioned 2.5 cm away from the sensor surface.

combinations of polynomial fields. We apply these matched rf fields in the context of stroboscopic phase-corrected spectral resolution[15] in the presence of various inhomogeneous fields.

We pick an ensemble that consists of identical molecules with three uncoupled spins. A static field inhomogeneity imparts a position dependence to the Larmór resonance of each nucleus and leads to a rapid loss of net signal. The spectrum, which is expected to show three resonances, is rendered featureless as a result of the inhomogeneous broadening. The method of B_0–B_1 matching[15] unwinds the phase dispersion, which has the effect of resurrecting the spectrum when a B_1 field is applied having the same position dependence as B_0. The correction pulses are implemented by applying the rapid sequence of composite pulses[30] followed by acquision of a point,

$$[\pi/2_{-y} - \beta_x - \pi/2_y - \text{delay} - \text{acquire}]_n. \tag{24}$$

The notation θ_ϕ indicates a rotation through θ radians about the ϕ axis in the xy plane, $\exp[-i\theta(I_x\cos\phi+I_y\sin\phi)]$. The sequence is written from left to right in time. The notation[7,31] $I_{x,y}$ denotes the Cartesian spin angular momentum operators summed over all the spins in the molecule. The $\pi/2$ pulses are created using the mean-square approximation to a uniform target field.

The nutation angle of the second pulse depends on position,

$$\beta(\mathbf{r}) = \gamma B_1(\mathbf{r})\tau_\beta, \tag{25}$$

where $B_1(\mathbf{r})$ is the position-dependent rf field estimated by the orthogonal projection method, τ_β is the pulse width which depends on the relative scaling between the B_0 and B_1 inhomogeneities. The spectrum is obtained by stroboscopically detecting the magnetization over multiple repetitions of the above sequence. This was done by calculating the evolution of the density matrix at each point in the grid and averaging over the volume. The free induction decay is given by

$$s(t) = \int_{\mathbf{r}\in\mathcal{V}} \mathrm{Tr}[U(\mathbf{r},t)\rho_0 U^{-1}(\mathbf{r},t)I^+]d^3\mathbf{r}, \tag{26}$$

where $I^+=I_1^+ + I_2^+ + I_3^+$ is the three-spin raising operator,[7] $\rho_0 = I_{1x}+I_{2x}+I_{3x}$ is the initial state and, $U(\mathbf{r},t)=\exp[-i\mathcal{H}(\mathbf{r})t] = \exp[-i\gamma B(\mathbf{r})I_z t]$ is the position dependent evolution operator. For the numerical simulation we discretize the time axis and replace the volume integral by the discrete sum over all points in $\mathcal{V}$. Results in this section were obtained using 128 points sampled using a dwell time of 200 μs.

The procedure is summarized as follows: (i) We are given a field inhomogeneity to be corrected, for example, $B_z=-gz$, $B_x=(g/2)\ y$, and $B_y=(g/2)\ x$ (this example is shown in Fig. 5). (ii) We obtain an optimal magnetic field $B_{1,x}$ whose target is proportional to the static field (here, $B_z=-gz$). (iii) Use this

TABLE II. Fidelities for Cartesian arrays of sizes 4×4, 6×6, and 8×8, and with Gaussian and flat kernels, $h(\mathbf{r})$. For the Gaussian kernel, the standard deviation of the Gaussian along each direction was set equal to 20% of the target volume side length. The corresponding fields and concomitant gradients are labeled in the same way as in Table I.

Label	4×4 Flat	6×6 Flat	8×8 Flat	4×4 Gauss.	6×6 Gauss.	8×8 Gauss.
A	0.9600	0.9897	0.9949	0.9972	0.9998	0.9999
B	0.8169	0.9516	0.9764	0.9823	0.9976	0.9985
C	0.8170	0.9517	0.9764	0.9823	0.9976	0.9985
D	0.9120	0.9512	0.9658	0.9879	0.9976	0.9989
E	0.7550	0.9252	0.9655	0.9427	0.9946	0.9979
F	0.7412	0.8726	0.9262	0.9025	0.9806	0.9958
G	0.8240	0.9248	0.9445	0.7740	0.9544	0.9849
H	0.5783	0.8930	0.9261	0.4338	0.9258	0.9718
I	0.5180	0.9057	0.9306	0.2472	0.8878	0.9498
J	0.5146	0.8253	0.8805	0.9267	0.9870	0.9860

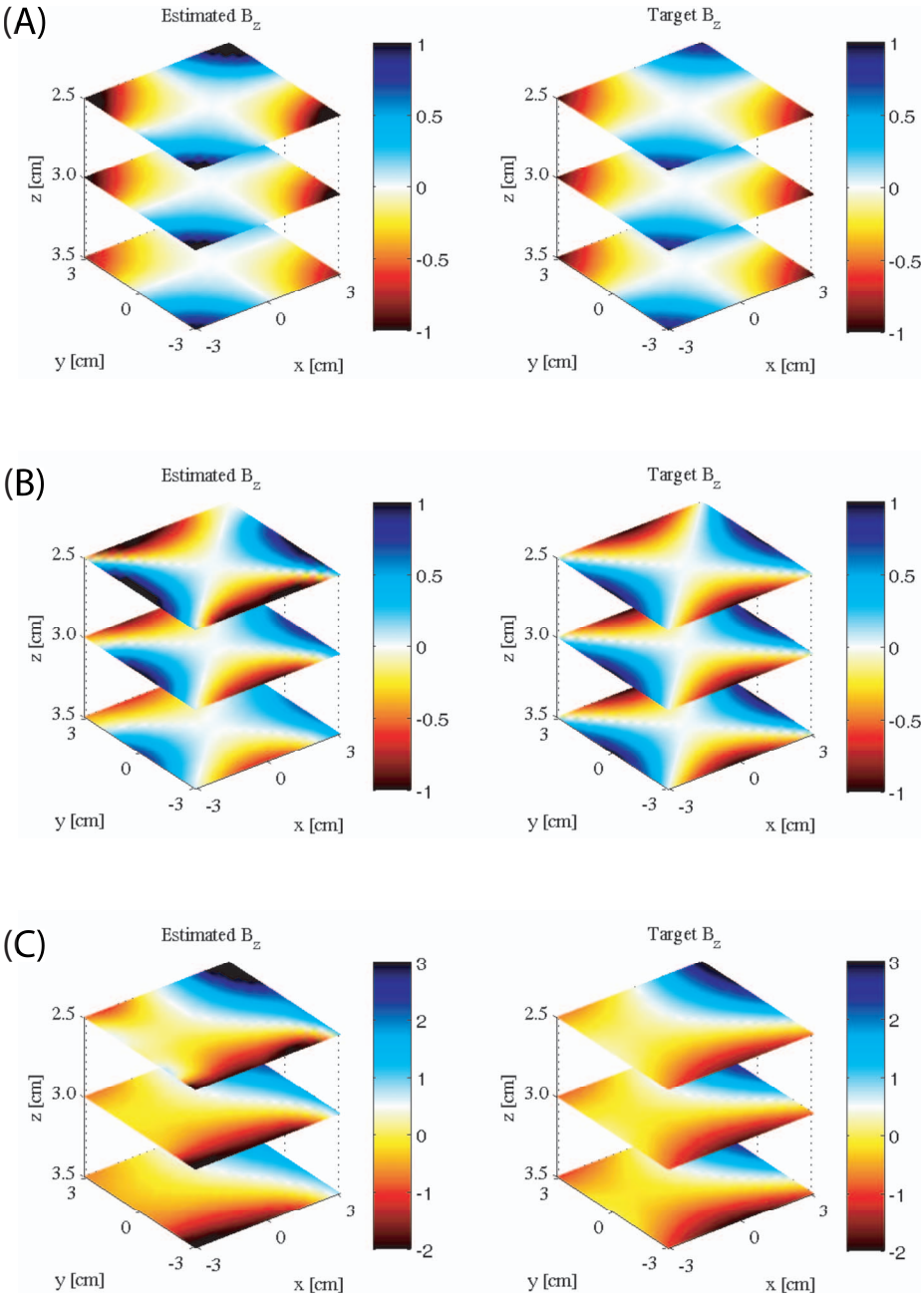

FIG. 4. (Color online) B_z component of field maps (estimated vs target) for an 8×8 Cartesian array of current loops calculated using the Gaussian kernel. Field maps are plots of $B_z(x,y,z)$ as xy slices taken at three planes, $z=2.5$, 3.0, and 3.5 cm for the following B_z component of target fields: (A) xy, (B) x^2-y^2, (C) $1+x+y-z+xy+(x^2-y^2)$.

synthesized field $B_{1,x}$ for the nutation operator of Eq. (24). (iv) The spectrum[45] is calculated using Eq. (26).

Figure 5 shows simulated spectra under conditions of resonance frequency of 42 MHz, chemical shift dispersion of 1.5 kHz, and inhomogeneities spanning the range 1–50 kHz. The ideal spectrum, perfectly counteracting the static inhomogeneity, $B_z\propto z$, is given in Fig. 5(a). The inhomogeneously broadened spectrum at 1 kHz is too wide to resolve individual spin resonances (figure not shown), but can be recovered by applying the corrective pulses using the mean-

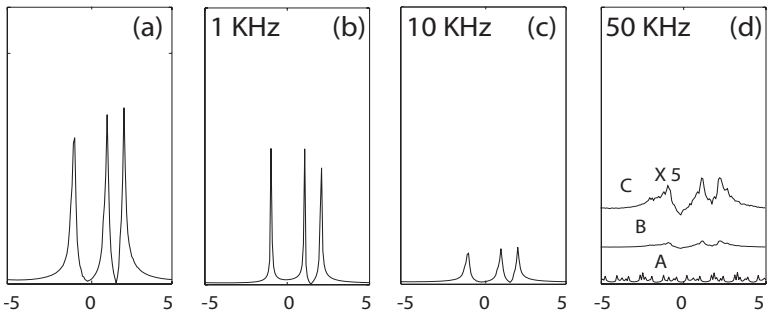

FIG. 5. Simulated spectra with the static field inhomogeneity $B_z\propto z$: (a) is the corrected spectrum with an ideal field that perfectly matches the inhomogeneity; (b), (c), and (d) are the corrected spectra at 1, 10, and 50 kHz; (d) A is the inhomogeneously broadened 50 kHz, B is the corrected spectrum, and C is B magnified five times. All spectra are drawn to the same vertical scale. The spectral width spans 10 kHz.

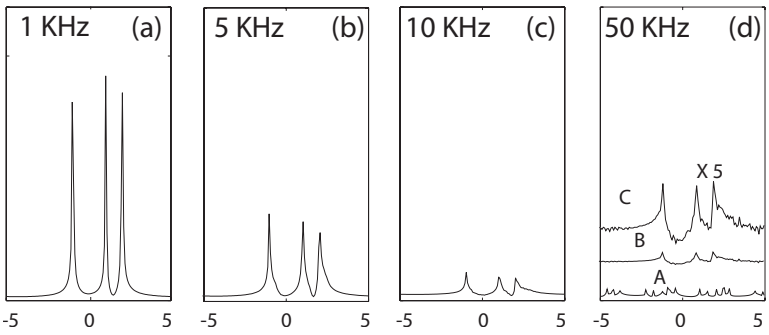

FIG. 6. Simulated spectra with the static field inhomogeneity $B_z \propto xy$: (a) is the corrected spectrum with an inhomogeneous broadening measure of 1 kHz; (b) is for a measure 5 kHz; (c) for 10 kHz; (d) A is the uncorrected spectrum at 50 kHz, B is the corrected spectrum, and C is B magnified five times. All spectra are drawn to the same vertical scale. The spectral width spans 10 kHz.

square estimator. The revived spectrum is presented in Fig. 5(b). Increasing the strength of the nonuniformity still preserves the spectral features quite well and the results are shown in Figs. 5(c) and 5(d) for 10 and 50 kHz. Even for inhomogeneities spanning 50 kHz, the recovered spectrum Fig. 5(d) B is still sharp, compared to the broadened featureless spectrum Fig. 5(d) A. The closeup in Fig. 5(d) C shows the three peaks distinctly.

The method performs well even in the case of a more complicated saddle gradient field whose target gradient field is $B_z = gxy$, $B_x = gyz$, and $B_y = gxz$. The simulated spectra are shown in Fig. 6. It is evident that the estimated field provides a very good match for the xy inhomogeneity up to frequencies of around 50 kHz, as shown in Eq. (6d): the three peaks are resolvable (B and C) and above the inhomogeneous spectrum shown in A. Likewise, our simulations for the other field inhomogeneity profiles given in Table I show similar improvements.

B. Quantal phase correction using static gradients

Another application of the target field method is the direct shimming of the static field nonuniformities. The disadvantage of this approach, of course, is that nonuniformities of the same magnitude must be created, whereas shimming rf pulse trains can be performed using weaker compensating nonuniformities (as long as the β pulses are applied long enough). Figure 7 shows comparisons of corrected vs uncorrected spectra obtained by target field shimming for a quadrupolar inhomogeneity whose target field was $B_z = -g(x^2 - y^2)$, $B_x = -g2xz$, and $B_y = g2yz$.

V. DISCUSSION

Given the high degree of fidelity that can be obtained in field matching, an immediate application of the target field method, aside from NMR, would be electromagnetic traps[4,5] that confine charged particles for mass spectroscopy,[32,33] optical and microwave spectroscopy,[34] and quantum computing.[35,36] The ideal Penning trap uses three hyperboloidal surfaces of revolution as electrodes for an ac electric field, and a homogeneous, axial magnetic field. These fields, respectively, confine the particle axially and radially. However, the magnetic field has two inevitable deviations from the ideal: the field may become inhomogeneous, and it may become misaligned from the axial direction. These nonidealities result in shifts of the eigenfrequencies and, moreover, the classical motion of the particle inside the trap also changes.[37] It is possible to use our approach of orthonormal fields as a compensating assembly for field adjustments. It may also be possible to use matched fields in the design of compensated sextupole fields for the magnetic confinement of neutral particles.[4,38]

There exists an approach[22] whereby amplitude-modulated static field gradients are applied during an adiabatic double passage to impart spatially dependent phase corrections. However, the double passage typically requires several milliseconds to apply and the method is not practical for high-speed applications. A more advanced method of parallel transmitter excitation, SENSE, exists which enables arbitrary three-dimensional magnetization modulation,[39] but is presently limited to long pulses and small-angle nutations. Application of our method to rf coil transmitter arrays requires methods to handle the mutual impedance[40] so that sources can be controlled independently. It should also be noted that wave propagation effects, as encountered in very high fields, are not accounted for in the mean-square estimation. Their inclusion would further complicate the analysis but should be straightforward.

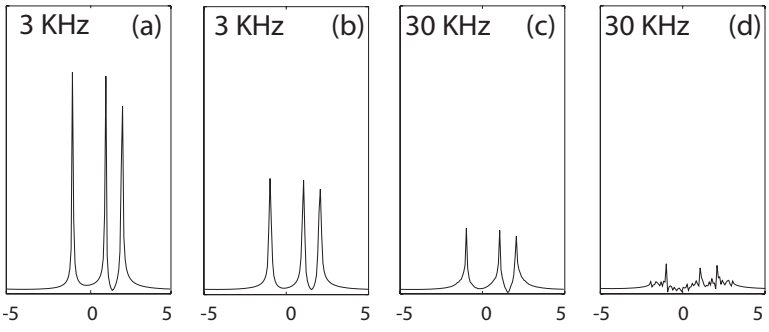

FIG. 7. Simulated spectra with the static field inhomogeneity $B_z \propto x^2 - y^2$: (a) is the shimmed spectrum with an inhomogeneous broadening measure of 3 kHz; (b) is the unshimmed spectrum; (c) is the shimmed spectrum for 30 kHz; (d) is the unshimmed spectrum. All spectra are drawn to the same vertical scale. The spectral width spans 10 kHz.

VI. CONCLUSIONS

We have demonstrated the potential of a simple mean-square estimator approach for synthesizing precise magnetic fields using a finite number of field sources, that are not necessarily orthogonal in the physical sense. Calculations demonstrate a flexible method for three-dimensional spatial manipulation of magnetic moments, and imparting desired corrections to the quantum spin phase during free evolution. This may lead to applications to electromagnetic trap design, nuclear magnetic resonance, and magnetic switching devices.

Higher-order rf gradient fields can be generated over a prescribed volume. Higher than 20-fold improvements in spectral resolution are possible. This enables the observation of spectral information in the presence of rapid inhomogeneity-induced quantum decoherence. Complementary to the rf field design, we have also shown the ability to generate static field gradients with high fidelity for improved magnet shimming. Finally, we showed the importance of rf concomitant gradients in high magnetic fields and how they affect generalized Euler rotations. We also pointed out the special cases where they can be justifiably ignored.

ACKNOWLEDGMENTS

This work was supported by the Director, Office of Science, Office of Basic Energy Sciences, Materials Sciences and Engineering Division, of the U.S. Department of Energy under Contract No. DE-AC03-76SF00098. We would like to thank Rennie Tang for help with the artwork and Ross D. Schlueter for useful discussions. We thank Alex Pines for many useful discussions and for encouraging this work.

APPENDIX A: GENERALIZED NUTATION FIELD MATCHING CONDITION

In the limit where all magnetic-field components must be matched, we may formulate a generalized condition for matched nutation as follows. Let $\mathcal{L}(t) \equiv \dot{\mathbf{r}}(t)$ be an integral curve of the vector field $\mathbf{B}_0(\mathbf{r})$ and $\dot{\mathcal{L}}$ be its time derivative. By definition of integral curve of a vector field,[41]

$$\dot{\mathcal{L}}(t) = \dot{\mathbf{r}}(t) \equiv \mathbf{B}_0[\mathbf{r}(t)]. \tag{A1}$$

Then, using the definition $\mathbf{B}_0[\mathbf{r}(t)] = \mathbf{B}_0 + \delta\mathbf{B}_0[\mathbf{r}(t)]$, this becomes

$$\dot{\mathcal{L}}(t) = \mathbf{B}_0 + \delta\mathbf{B}_0[\mathbf{r}(t)] \tag{A2}$$

Using the chain rule $d\mathbf{B}[\mathbf{r}(t)]/dt = (\dot{\mathbf{r}} \cdot \nabla)\mathbf{B}[\mathbf{r}(\mathbf{t})]$, the second derivative $\ddot{\mathcal{L}}$ is given by

$$\ddot{\mathcal{L}}(t) = (\mathbf{B}_0 \cdot \nabla)\delta\mathbf{B}_0[\mathbf{r}(t)] + \{\delta\mathbf{B}_0[\mathbf{r}(t)] \cdot \nabla\}\delta\mathbf{B}_0[\mathbf{r}(t)], \tag{A3}$$

is perpendicular to $\mathbf{B}_0$. Therefore the resulting vector field can be used for localized spin excitation. Similarly, the vector field $\dot{\mathcal{L}} \times \ddot{\mathcal{L}}$ is perpendicular to $\mathbf{B}_0$ and may serve as a nutation field. Then, $\frac{\dot{\mathcal{L}} \times \ddot{\mathcal{L}}}{|\dot{\mathcal{L}} \times \ddot{\mathcal{L}}|}$ gives the unit vector pointing in this direction. Scaling the unit vector by the local magnitude of the static field gives a nutation field proportional to the local magnitude of the static field throughout the volume. Thus the relation

$$\mathbf{B}_1(\mathbf{r}) \propto |\dot{\mathcal{L}}| \frac{\ddot{\mathcal{L}} \times \dot{\mathcal{L}}}{|\ddot{\mathcal{L}} \times \dot{\mathcal{L}}|} \tag{A4}$$

holds, up to a constant. This condition is completely general and its use is not specific or limited to NMR.

APPENDIX B: NULLING OF CONCOMITANT COMPONENTS

There exist many possible ways of constructing polynomial magnetic vector fields with desired components. The most simple method is by constructing magnetic fields of the form (up to a scaling factor and dc offset),

$$\underline{B}^*_{xy} \equiv B_x - iB_y = (x + iy)^n e^{i\delta}, \tag{B1}$$

$$\underline{B}^*_{xz} \equiv B_x - iB_z = (x + iz)^n e^{i\delta}, \tag{B2}$$

$$\underline{B}^*_{yz} \equiv B_y - iB_z = (y + iz)^n e^{i\delta}, \tag{B3}$$

where $n \in \mathbb{N}$ is the degree of the monomial and $\delta \in \mathbb{R}$ is a phase angle. These fields not only satisfy Maxwell's equations, but have the nice property that their third, unspecified component is constant. This is useful for enforcing the nulling of concomitant fields along a certain direction. For example, $\underline{B}^*_{xy}$ is a magnetic field with nonzero x and y components and a null z component, $B_z = 0$. Such fields have been physically realized using harmonic corrector rings.[42,43]

*lsbouchard@lbl.gov; URL: http://waugh.cchem.berkeley.edu

[1] *Spin Dynamics in Confined Magnetic Structures II*, Topics in Applied Physics, edited by B. Hildebrands and K. Ounadjela (Springer, Berlin, Heidelberg, 2003).

[2] *Spin Dynamics in Confined Magnetic Structures I*, Topics in Applied Physics, edited by B. Hildebrands and K. Ounadjela (Springer, Berlin, Heidelberg, 2001).

[3] *Spin Dynamics in Confined Magnetic Structures III*, Topics in Applied Physics, edited by B. Hildebrands and K. Ounadjela (Springer, Berlin, Heidelberg, 2006).

[4] Wolfgang Paul, Rev. Mod. Phys. **62**, 531 (1990).

[5] F. G. Major, V. N. Gheorghe, and G. Werth, *Charged Particle Traps* (Springer-Verlag, Berlin, 2005).

[6] M. G. E. Golay, Rev. Sci. Instrum. **29**, 313 (1958).

[7] R. R. Ernst, G. Bodenhausen, and A. Wokaun, *Principles of Nuclear Magnetic Resonance in One and Two Dimensions*

(Clarendon Press, Oxford, 1987).
[8] A. Abragam, *Principles of Nuclear Magnetism* (Oxford, New York, 1983).
[9] J. Perlo, F. Casanova, and B. Blümich, J. Magn. Reson. **180**, 274 (2006).
[10] J. Perlo, F. Casanova, and B. Blümich, Science **315**, 1110 (2007).
[11] J. Perlo, V. Demas, F. Casanova, C. A. Meriles, J. Reimer, A. Pines, and B. Blümich, Science **308**, 1279 (2005).
[12] A. Wiesmath, C. Filip, D. E. Demco, and B. Blümich, J. Magn. Reson. **144**, 60 (2002).
[13] J. Perlo, F. Casanova, and B. Blümich, J. Magn. Reson. **176**, 64 (2005).
[14] J. Perlo, F. Casanova, and B. Blümich, J. Magn. Reson. **173**, 254 (2005).
[15] C. A. Meriles, D. Sakellariou, H. Heise, A. J. Moulé, and A. Pines, Science **293**, 82 (2002).
[16] D. G. Norris and J. M. S. Hutchison, Magn. Reson. Imaging **8**, 33 (1990).
[17] P. L. Volegov, J. C. Mosher, M. A. Epsy, and R. H. Kraus, Jr., J. Magn. Reson. **175**, 103 (2005).
[18] D. A. Yablonskiy, A. L. Sustanskii, and J. J. Ackerman, J. Magn. Reson. **174**, 279 (2005).
[19] M. P. Augustine, A. Wong-Foy, J. L. Yarger, M. Tomaselli, A. Pines, D. M. TonThat, and J. Clarke, Appl. Phys. Lett. **72**, 1908 (1998).
[20] C. A. Meriles, D. Sakellariou, A. H. Trabesinger, V. Demas, and A. Pines, Proc. Natl. Acad. Sci. U.S.A. **102**, 1840 (2005).
[21] L.-S. Bouchard, Phys. Rev. B **74**, 054103 (2006).
[22] D. Topgaard, R. W. Martin, D. Sakellariou, C. A. Meriles, and A. Pines, Proc. Natl. Acad. Sci. U.S.A. **101**, 17576 (2004).
[23] V. Demas, D. Sakellariou, C. A. Meriles, S. Han, J. Reimer, and A. Pines, Proc. Natl. Acad. Sci. U.S.A. **101**, 8845 (2004).
[24] P. T. Callaghan, *Principles of Nuclear Magnetic Resonance Microscopy* (Clarendon Press, Oxford, 1991).
[25] J. J. Sakurai, *Modern Quantum Mechanics* (Addison-Wesley Publishing Company, Reading, MA, 1994).
[26] R. Raulet, D. Grandclaude, F. Humbert, and D. Canet, J. Magn. Reson. **124**, 259 (1997).
[27] D. Canet, Prog. Nucl. Magn. Reson. Spectrosc. **30**, 101 (1997).
[28] D. Canet, B. Diter, A. Belmajdoub, J. Brondeau, J.-C. Boubel, and K. Elbayed, J. Magn. Reson. (1969-1992) **81**, 1 (1989).
[29] M. E. Rose, *Elementary Theory of Angular Momentum* (John Wiley and Sons, Inc., London 1957).
[30] R. Freeman, T. A. Frenkiel, and M. Levitt, J. Magn. Reson. (1969-1992) **44**, 409 (1981).
[31] O. W. Sørensen, G. W. Eich, M. H. Levitt, G. Bodenhausen, and R. R. Ernst, Prog. Nucl. Magn. Reson. Spectrosc. **16**, 163 (1983).
[32] O. J. Orient, A. Chutijan, and V. Garkanian, Rev. Sci. Instrum. **68**, 1393 (1997).
[33] R. E. March and J. F. Todd, *Quadrupole Ion Trap Mass Spectrometry*, 2nd ed. (Wiley-Interscience, New York, 2005).
[34] W. H. Oskay, S. A. Diddams, E. A. Donley, T. M. Fortier, T. P. Heavner, L. Hollberg, W. M. Itano, S. R. Jefferts, M. J. Delaney, K. Kim, F. Levi, T. E. Parker, and J. C. Bergquist, Phys. Rev. Lett. **97**, 020801 (2006).
[35] J. I. Cirac and P. Zoller, Phys. Rev. Lett. **74**, 4091 (1995).
[36] D. Stick, W. K. Hensinger, S. Olmschenk, M. J. Madsen, K. Schwab, and C. Monroe, Nat. Phys. **2**, 36 (2006).
[37] L. S. Brown and G. Gabrielse, Phys. Rev. A **25**, 2423 (1982).
[38] M. B. H. Breese and D. N. Jamiesen, Nucl. Instrum. Methods Phys. Res. B **104**, 81 (1995).
[39] P. Ullmann, S. Junge, M. Wick, F. Seifert, W. Ruhm, and J. Hennig, Magn. Reson. Med. **54**, 994 (2005).
[40] S. M. Wright and L. L. Wald, NMR Biomed. **10**, 394 (1997).
[41] M. Spivak, *A Comprehensive Introduction to Differential Geometry*, Vol. 1, 3rd ed. (Publish or Perish, Houston, 1999).
[42] R. D. Schlueter, D. Humphries, and J. Watanabe, Nucl. Instrum. Methods Phys. Res. A **395**, 153 (1997).
[43] R. C. Jachmann, D. R. Trease, L.-S. Bouchard, D. Sakellariou, R. W. Martin, R. D. Schlueter, T. F. Budinger, and A. Pines, Rev. Sci. Instrum. **78**, 035115 (2007).
[44] The geometric interpretation is an orthogonal projection of the target field $\mathbf{B}$ into the vector space $\mathcal{L}\{\mathbf{B}_1, \ldots, \mathbf{B}_n\}$ spanned by the available physical field sources.
[45] For simplicity, we display all spectra in magnitude mode, which is sufficient to illustrate the effects of phase decoherence over a volume.